

# Accepted Manuscript

## Article

Fabrication of Periodic Nanostructures Using AFM Tip-Based Nanomachining: Combining Groove and Material Pile-Up Topographies

Yanquan Geng, Yongda Yan, Jiqiang Wang, Emmanuel Brousseau, Yanwen Sun, Yazhou Sun

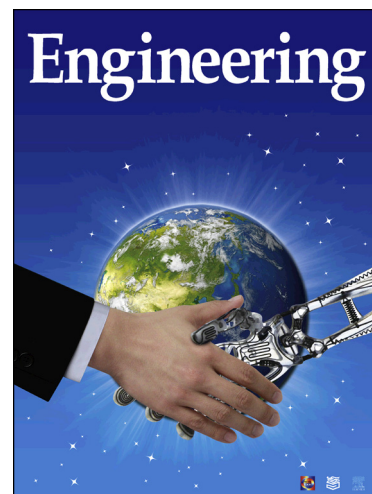
PII: S2095-8099(18)30405-3  
DOI: <https://doi.org/10.1016/j.eng.2018.09.010>  
Reference: ENG 132

To appear in: *Engineering*

Received Date: 28 April 2018  
Revised Date: 15 June 2018  
Accepted Date: 18 September 2018

Please cite this article as: Y. Geng, Y. Yan, J. Wang, E. Brousseau, Y. Sun, Y. Sun, Fabrication of Periodic Nanostructures Using AFM Tip-Based Nanomachining: Combining Groove and Material Pile-Up Topographies, *Engineering* (2018), doi: <https://doi.org/10.1016/j.eng.2018.09.010>

This is a PDF file of an unedited manuscript that has been accepted for publication. As a service to our customers we are providing this early version of the manuscript. The manuscript will undergo copyediting, typesetting, and review of the resulting proof before it is published in its final form. Please note that during the production process errors may be discovered which could affect the content, and all legal disclaimers that apply to the journal pertain.



## Research

## Precision Engineering—Article

**Fabrication of Periodic Nanostructures Using AFM Tip-Based Nanomachining: Combining Groove and Material Pile-Up Topographies**Yanquan Geng<sup>a,b</sup>, Yongda Yan<sup>a,b,\*</sup>, Jiqiang Wang<sup>b</sup>, Emmanuel Brousseau<sup>c,\*</sup>, Yanwen Sun<sup>b</sup>, Yazhou Sun<sup>b</sup><sup>a</sup> Key Laboratory of Micro-systems and Micro-structures Manufacturing, Ministry of Education, Harbin Institute of Technology, Harbin 150001, China<sup>b</sup> Center for Precision Engineering, Harbin Institute of Technology, Harbin 150001, China<sup>c</sup> Cardiff School of Engineering, Cardiff University, Cardiff CF24 3AA, UK

\* Corresponding authors.

E-mail address: yanyongda@hit.edu.cn (Y. Yan), BrousseauE@cardiff.ac.uk (E. Brousseau)

**ARTICLE INFO***Article history:*

Received 27 April 2018

Revised 14 June 2018

Accepted 15 June 2018

Available online

*Keywords:*

Atomic force microscopy

Nanomachining

Periodic nanostructure

Single-crystal copper

**ABSTRACT**

This paper presents an atomic force microscopy (AFM) tip-based nanomachining method to fabricate periodic nanostructures. This method relies on combining the topography generated by machined grooves with the topography resulting from accumulated pile-up material on the side of these grooves. It is shown that controlling the distance between adjacent and parallel grooves is the key factor in ensuring the quality of the resulting nanostructures. The presented experimental data show that periodic patterns with good quality can be achieved when the feed value between adjacent scratching paths is equal to the width between the two peaks of material pile-up on the sides of a single groove. The quality of the periodicity of the obtained nanostructures is evaluated by applying one- and two-dimensional fast Fourier transform (FFT) algorithms. The ratio of the area of the peak part to the total area in the normalized amplitude–frequency characteristic diagram of the cross-section of the measured AFM image is employed to quantitatively analyze the periodic nanostructures. Finally, the optical effect induced by the use of machined periodic nanostructures for surface colorization is investigated for potential applications in the fields of anti-counterfeiting and metal sensing.

## 1. Introduction

The rapid development of nanotechnology-based devices has led to periodic nanostructures being widely relied on for a range of applications including the design of solar cells [1,2], nanoscale plasmonic structures [3–5], and the structural coloration of metallic surfaces [6,7]. However, the controlled fabrication of periodic nanostructures with specific dimensions still presents important challenges. Researchers have used several methods to produce periodic nanostructures, including nanoimprint lithography [8], focused ion-beam milling [9], direct mechanical machining [10], and electrochemical machining [11]. However, these methods are usually associated with complicated operations, low throughput, low machining accuracy, and/or significant implementation cost. Therefore, the development of a manufacturing approach to fabricate periodic nanostructures with accurate dimensions is still an area of important research interest.

The atomic force microscopy (AFM) tip-based nanofabrication technique has been shown to be an attractive alternative to achieve one-dimensional (1D), two-dimensional (2D), and even three-dimensional (3D) nanostructures successfully [12–15]. In particular, for the fabrication of 3D nanostructures, several AFM tip-based nanomachining approaches have been proposed, such as thermochemical lithography [16], local anodic oxidation [17], tribochemistry-induced etching [18], and nanomechanical machining [19]. Among these, the nanomechanical machining method has the advantages of being readily implemented and being the most flexible means of fabricating 3D nanostructures. It is reasonable to assume that if a method has been proven to be suitable for generating 3D nanostructures, it could be further employed to produce periodic nanostructures. In this context, researchers have already attempted to implement tip-based nanomechanical machining to fabricate sinusoidal periodic nanostructures [19–22]. We [19] first proposed the integration of a closed-loop nanoscale precision stage with an AFM in order to mechanically fabricate such surface topographies. However, in our study, the dimensions of the nanostructures could not be determined before machining. To help overcome this issue, we [20] developed a theoretical model to reveal the relationship between the normal load and the machined depth. Based on this model, the normal load could be predicted in order to achieve the expected nanostructure dimensions. Moreover, it was concluded in numerous previous studies [20,23,24] that the machined depth is not only dependent on the applied normal load, but also influenced by the feed value during the scratching process. Thus, keeping the normal load constant during the machining process and enabling the feed to be varied in order to control the machined depth were subsequently considered [21,22]. This method could be implemented to machine large-scale periodic nanostructures on the radial face of axisymmetric components, and to improve the processing efficiency of the AFM tip-based machining technique. However, it was noticed that the slope of the fabricated structures had to be restricted to a range from  $-12^\circ$  to  $12^\circ$ , in order to guarantee a machining error within 10%. This means that for a given amplitude of the structure, the period cannot be less than a limiting value [21]. For example, if the desired amplitude is 125 nm, then the minimum value of the period for the sinusoidal waveforms is  $3.74\ \mu\text{m}$ . This is an important limitation of the “milling-like” machining mode, despite the possibility of generating periodic nanostructures with it. Recently, a method was proposed by He et al. [25] to fabricate arrays of grooves with a period of 30 nm. In that case, dynamic plowing lithography was employed to scratch a polymer thin film. However, it was difficult to obtain an amplitude greater than 20 nm due to the limitation in the energy input by the tip; in addition, there were issues with understanding the specific material-removal mechanism in that study. It is important to note that material accumulation in the form of pile-ups on the sides of the machined grooves was a key factor in the study reported by He et al. [25]. We have found that the static machining method can also be used to scratch single-crystal copper, and that it is accompanied by the formation of material pile-up along certain scratching directions. Interestingly, the amplitude between the top of a pile-up and the bottom of a groove can reach a relatively large range [26]. Thus, we argue that conventional (i.e., static) AFM tip-based nanomachining can be suitable for the fabrication of periodic nanostructures by implementing a “combined writing” approach. More specifically, we propose that the topography generated by the machined grooves and the topography resulting from the pile-up formation can be combined, leading to the manufacture of controlled periodic nanostructures.

In this study, the AFM tip-based static machining method is used to fabricate nanostructures by means of the proposed “combined writing” approach on a single-crystal copper surface. The periodicity of the obtained nanostructures is evaluated by 1D and 2D fast Fourier transform (FFT) algorithms. Finally, the colorization of the machined periodic nanostructure is examined.

## 2. Experiments

### 2.1. Experimental setup

A commercial AFM (Dimension Icon, Bruker, Germany) was employed in this study. The NanoMan module of this AFM system was selected to conduct all the scratching operations. In this module, the scratching trajectory of the AFM tip is controlled by a piezoelectric tube (PZT), and the maximum motion ranges of the PZT in the  $x$  and  $y$

directions are  $90\ \mu\text{m}$  and  $90\ \mu\text{m}$ , respectively. To avoid tip wear during the scratching process, a diamond AFM tip (PDNISP, Bruker, Germany) was selected. The cantilever of this diamond tip is made of stainless steel, and its calibrated spring constant is given as  $275\ \text{N}\cdot\text{m}^{-1}$  by the manufacturer. The radius of this diamond tip was evaluated as  $110\ \text{nm}$  using the tip blind-reconstruction method [27]. The sample used in this study was single-crystal copper with a (110) crystallographic plane (Hefei Ke Jing Materials Technology Co., Hefei, China). Prior to its delivery, the sample was polished by the manufacturer to a resulting roughness ( $R_a$ ) less than  $5\ \text{nm}$ , as measured with tapping-mode AFM. The radius of the diamond tip was assumed to be constant during the scratching process due to the much higher hardness of the diamond compared with the softer copper sample. After machining, the obtained nanostructures were measured by a silicon nitride tip with a normal spring constant of  $0.35\ \text{N}\cdot\text{m}^{-1}$  in contact-mode AFM. Before both the machining and the imaging steps, the sample was ultrasonically cleaned in alcohol solution for  $10\ \text{min}$ .

## 2.2. Methodology

According to our previous study [26], material accumulates on the sides of the grooves in the form of pile-up when single-crystal copper with a (110) crystallographic plane is scratched using an AFM diamond tip. In that study, the “edge-forward” direction was employed as the scratching direction. Material pile-ups form on both sides of the groove with this selected scratching direction [28]. As discussed in the Introduction, the approaches utilized in previous studies to achieve periodic nanostructures by controlling the applied normal load and the feed value were relatively time-consuming and were limited by a minimum achievable period of around  $2\ \mu\text{m}$ . For these reasons, we propose a novel and simple AFM tip-based nanomechanical machining method to fabricate such nanostructures. Our method relies on the combination of material accumulation and the machined groove, as shown in Fig. 1. The detailed realization of the machining process of one periodic nanostructure is described as follows:

**Step 1:** The diamond AFM tip approaches the sample surface until a preset normal load is attained. This normal load is subsequently kept constant by the feedback loop of the AFM system during the machining process. The diamond tip is controlled by the PZT of the AFM system in order to scratch the sample surface to achieve one groove. The length of the machined groove is used to control the width of the periodic nanostructure.

**Step 2:** After a groove is machined, the diamond AFM tip is moved to the start point of the subsequent groove by tapping mode in order to avoid destroying the sample surface during the repositioning of the tip. This new groove is cut parallel to the previous one and the offset distance is precisely controlled in order to make the adjacent material pile-ups of these two machined grooves combine into one peak. The offset distance between the adjacent machined grooves is defined as the feed value in this study. The feed value should be evaluated based on the relationship between the normal load and the total width of the machined groove.

**Step 3:** Step 2 is repeated until the machining process of the periodic nanostructure is completed, as shown in Fig. 1(b). The sum of the feed values is utilized to determine the length of the period nanostructure.

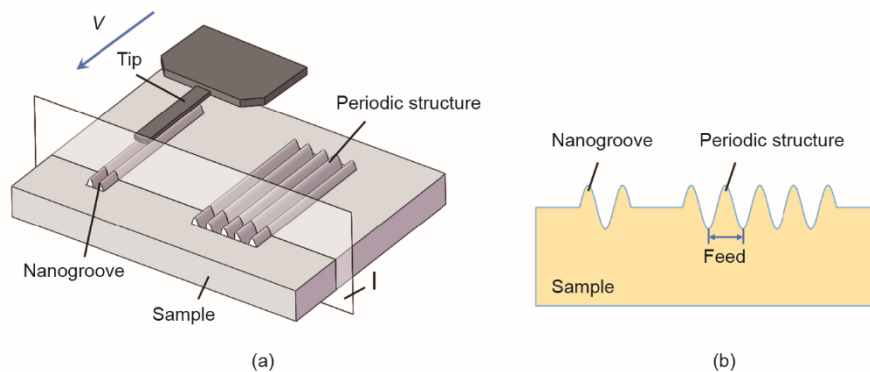


Fig. 1. (a) Schematic of the machining principle employed to generate periodic nanostructures; (b) cross-section of plane I.

## 3. Results and discussion

### 3.1. Relationship between the feed and the total width of the groove

As mentioned above, the feed value is chosen according to the total width of the groove, which is related to the applied normal load. Thus, the relationship between the applied normal, the machined depth, and the total width of the groove should be investigated first. Fig. 2 shows an AFM image and the corresponding cross-section of a typical nanogroove machined with a normal load of  $120\ \mu\text{N}$  and a scratching speed of  $3\ \mu\text{m}\cdot\text{s}^{-1}$ . The total width of the groove is defined as the period of the groove, which is the distance between the two peaks of material pile-up on both sides of the grooves, as shown in Fig. 2 (b). The sum of the height of the material pile-up and the machined depth is defined

as the amplitude of the structure. To study the relationship between the profile of the machined groove and the applied normal load, eight nanogrooves were machined on a (110) single-crystal copper surface with normal loads from 80 to 150  $\mu\text{N}$  and a fixed scratching velocity of  $3 \mu\text{m}\cdot\text{s}^{-1}$ . Fig. 3 shows the experimental relationship between the machined depth, amplitude, period, and applied normal load. It can be observed that the machined depth of the grooves ranges from 180 to 300 nm, while the amplitude is almost twice the value of the machined depth. The achieved period ranges from about 1.1 to 1.6  $\mu\text{m}$ . Based on these results, a polynomial fitting was used to describe these relationships, as expressed in Eqs. (1–3).

$$y_1 = 22.4857 + 2.20685x - 0.00245x^2 \quad (1)$$

$$y_2 = 21.61512 + 5.03543x - 0.00874x^2 \quad (2)$$

$$y_3 = 0.33705 + 0.01059x - 0.0000135119x^2 \quad (3)$$

where  $y_1$ ,  $y_2$ , and  $y_3$  represent the machined depth, amplitude, and period of the grooves, respectively, and  $x$  is the applied normal load. The fitted curves are shown in Fig. 3.

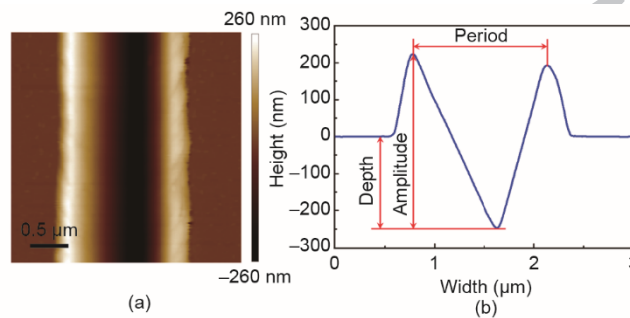


**Fig. 2.** (a) AFM image and (b) corresponding cross-section of a typical groove machined with a normal load of 120  $\mu\text{N}$  and a scratching speed of  $3 \mu\text{m}\cdot\text{s}^{-1}$ .

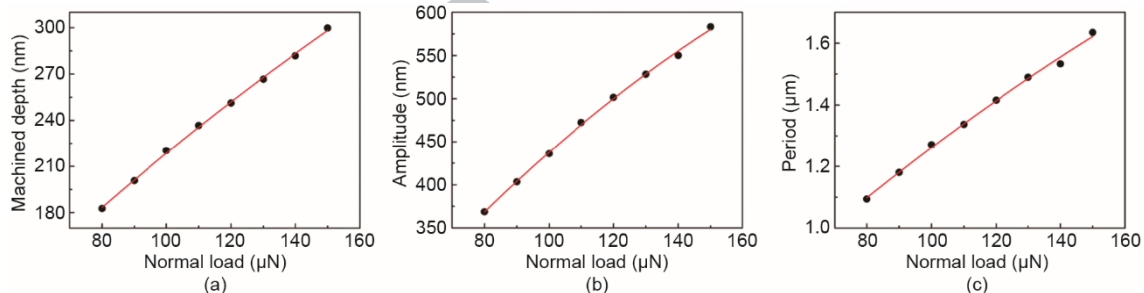


**Fig. 3.** (a) Machined depth, (b) amplitude, and (c) period of the scratched grooves as a function of the normal load and fitted second-order polynomials.

Next, a normal load of 150  $\mu\text{N}$  was selected in order to study the relationship between the feed and the total width of the groove—that is, the period of the groove—in the case of machining two adjacent parallel grooves. From Eq. (3), the period of the groove can be calculated as 1.635  $\mu\text{m}$ . Four feed values were chosen to conduct the experimental tests: 0.25  $\mu\text{m}$ , 0.75  $\mu\text{m}$ , 1.635  $\mu\text{m}$ , and 2  $\mu\text{m}$ . The AFM images of the machined structures and the corresponding cross-sections are shown in Fig. 4. It can be observed that only one groove can be obtained when scratching with a feed value of 0.25  $\mu\text{m}$ . A possible reason is that the feed value in this case is too close to the radius of the AFM tip (about 0.11  $\mu\text{m}$  in this study), so the second scratching path simply ends up overlapping the previous machining trajectory. For a feed of 0.75  $\mu\text{m}$ , although this value is smaller than the total width of the groove, it is much larger than the radius of the tip. Thus, as shown in Fig. 4(b), the resulting adjacent scratch paths are separated from each other. Due to the overlapping of the adjacent scratched groove, the height of the left side of material pile-up for the second groove is smaller than that of the previous machined groove. When the feed value is larger than the total width of the groove, which was selected as 2  $\mu\text{m}$  in this study, the adjacent scratch paths are not overlapped, as shown in Fig. 4(c). It can be further observed that there is a small gap between the two material pile-ups for the adjacent machined grooves. Due to the limitation of the geometrical size of the AFM tip, this gap cannot be accurately measured by the traditional AFM scanning process. Finally, a feed value equal to the total width of the groove (i.e., 1.635  $\mu\text{m}$ ) was selected to conduct the scratching test. The corresponding AFM image of the machined groove is shown in Fig. 4(d). In this case, the adjacent material pile-ups can exactly connect with each other and a regular periodicity is observed. Moreover, the height of the combined material pile-up is slightly larger than that achieved

with single-groove scratching. This is probably because the material volume of the combined pile-up is larger than the material accumulation generated for a single groove.

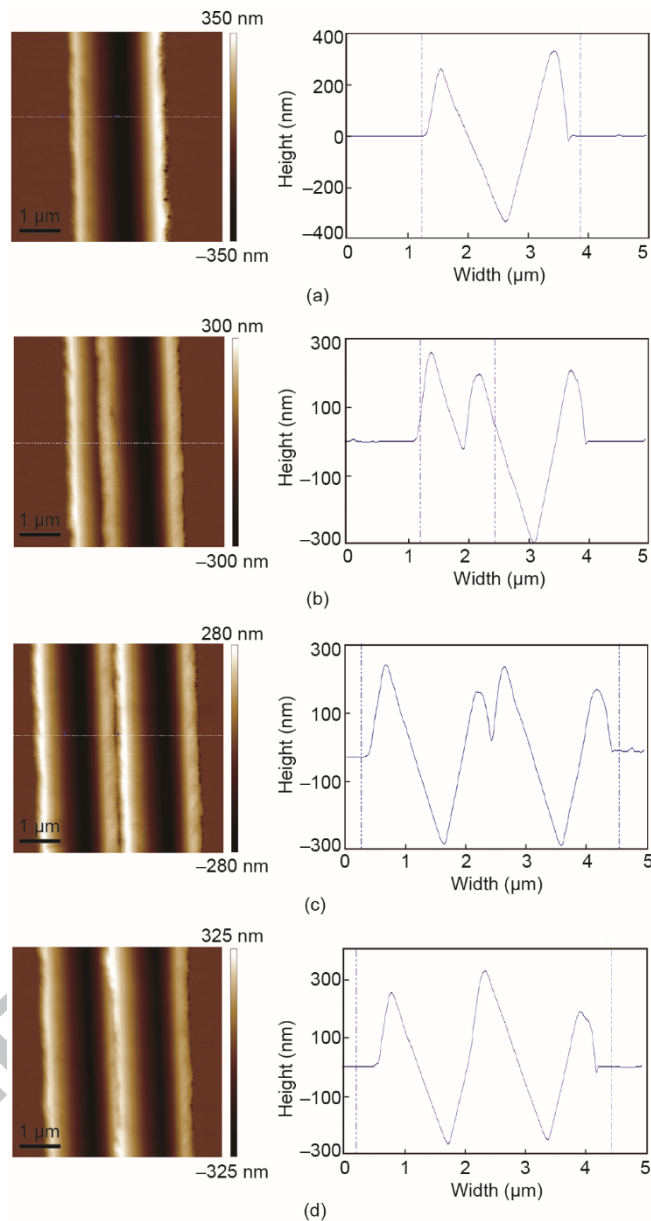


**Fig. 4.** (Left column) AFM images of machined structures when scratching two adjacent and parallel grooves, and (right column) corresponding cross-sections for feed values of (a)  $0.25 \mu\text{m}$ , (b)  $0.75 \mu\text{m}$ , (c)  $2 \mu\text{m}$ , and (d)  $1.635 \mu\text{m}$ .

We also fabricated additional periodic nanostructures, this time with a greater number of parallel grooves. In this case, a normal load of  $100 \mu\text{N}$  and a scratching velocity of  $3 \mu\text{m}\cdot\text{s}^{-1}$  were selected. Using Eq. (3), the total width of the groove was predicted to be  $1.271 \mu\text{m}$ . Therefore,  $0.5 \mu\text{m}$ ,  $0.75 \mu\text{m}$ ,  $1.271 \mu\text{m}$ , and  $1.5 \mu\text{m}$  were chosen as the feed values for these nanoscratching tests. The AFM images and corresponding cross-sections are shown in Fig. 5, with the results for the feeds of  $0.5 \mu\text{m}$  and  $0.75 \mu\text{m}$  being shown in Fig. 5(a) and (b), respectively. Similar to the situation shown in Fig. 4(b), these two feed values are smaller than the total width of a single scratched groove but much larger than the radius of the AFM tip. These two figures show that processed materials can fill the previous scratching path and thereby reduce the amplitude of the periodic structures. In addition, due to material filling the previous groove, the structure is mainly above the sample surface. For the feed value of  $0.5 \mu\text{m}$ , the amplitude and period of the machined structures are around  $100 \text{ nm}$  and  $500 \text{ nm}$ , respectively, while for the feed value of  $0.75 \mu\text{m}$ , the amplitude and period are around  $150 \text{ nm}$  and  $730 \text{ nm}$ . The relatively larger amplitude of the structure that was machined with the feed value of  $0.75 \mu\text{m}$  could be due to a larger volume of material being filled in the previous groove as a consequence of the increased feed. From the cross-sections, it can be observed that a groove with a significant depth

of around 190 nm can be generated on the right side of the periodic structure for both cases. This is because it is the last groove to be machined in a single periodic structure. Moreover, nanostructures that are much smaller than the initial groove can be obtained by using a relatively smaller feed. Fig. 5(c) shows the periodic structure that is fabricated by using a feed equal to the total width of the initial groove—that is, 1.271  $\mu\text{m}$ . It can be seen that a more consistent amplitude and period for the structure can be achieved in this case. The amplitude is around 390 nm and the ridges on both extremities of the structure are slightly lower than the ridges in the other cases. The same result was observed in the previous experiments with only two grooves.

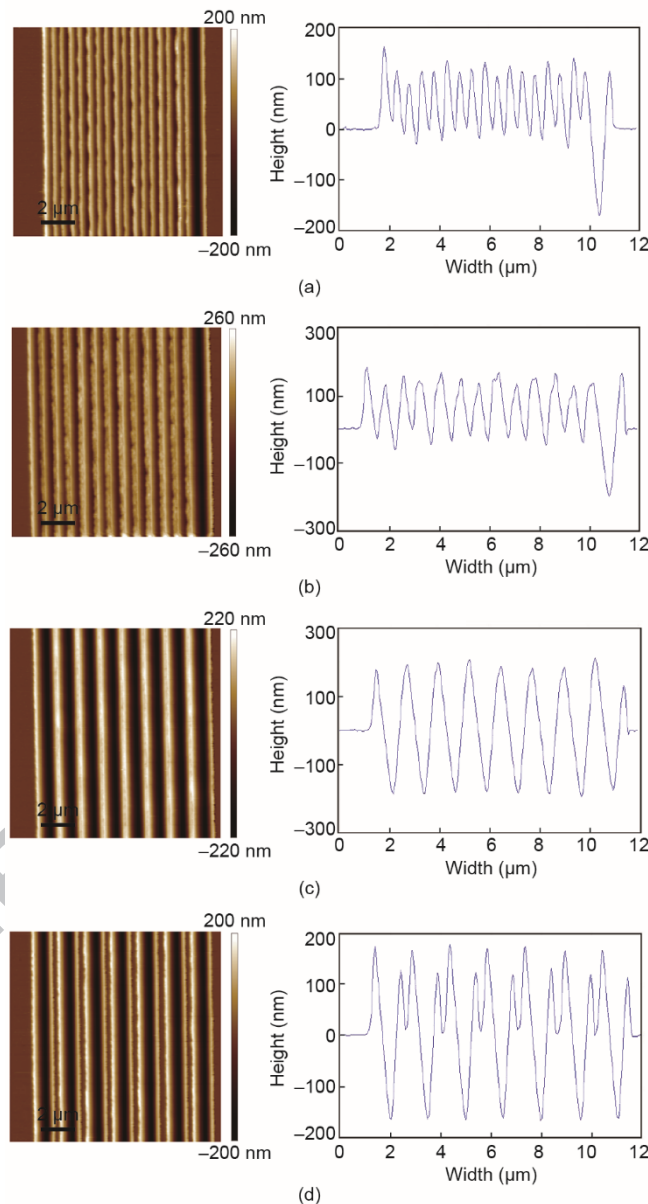


**Fig. 5.** (Left column) AFM images of the machined periodic structures and (right column) corresponding cross-sections for feed values of (a) 0.5  $\mu\text{m}$ , (b) 0.75  $\mu\text{m}$ , (c) 1.27  $\mu\text{m}$ , and (d) 1.5  $\mu\text{m}$ .

### 3.2. Evaluation of the periodicity of the machined nanostructures

In order to evaluate the periodicity of the machined nanostructures, the 2D FFT approach was applied to the AFM images using the Spectrum 2D module of the commercial software Nanoscope Analysis from Bruker. Fig. 6 shows the 2D FFT results for the machined structures described in Fig. 5. It can be observed from the 2D FFT results that the bright lines are perpendicular to the horizontal and vertical directions, which results from the striated structure. As shown in Fig. 6(a–c), there are two main bright lines on both sides of the central point of the image, which are vertical. This indicates that the power spots are mainly concentrated on only one spectrum and that the machined structures mainly comprise a waveform with a single spectral signature. The power spots are more concentrated for

the 2D FFT of the structure machined with a feed value of 1.27  $\mu\text{m}$ , compared with those obtained for the structures scratched with feed values of 0.5  $\mu\text{m}$  and 0.75  $\mu\text{m}$ . This means that the structure machined with a feed value of 1.27  $\mu\text{m}$  shows better periodicity. Moreover, the distance between the bright line and the central point of the 2D FFT image decreases as the feed value increases in the range from 0.5 to 1.27  $\mu\text{m}$ . This means that the period of the structure increases with an increase in feed value—a finding that agrees well with the earlier discussion of the cross-sections shown in Fig. 5. For the 2D FFT image of the structure machined with a feed value of 1.5  $\mu\text{m}$ , three obvious bright lines can be seen on both sides of the central point of the image. This indicates that the machined structure comprises waveforms with several spectral signatures.

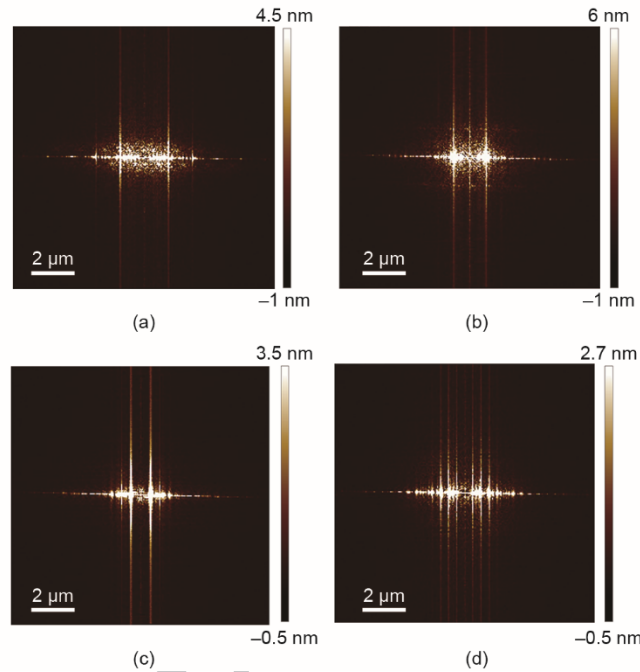


**Fig. 6.** 2D FFT results of the periodic nanostructures machined using feed values of (a) 0.5  $\mu\text{m}$ , (b) 0.75  $\mu\text{m}$ , (c) 1.27  $\mu\text{m}$ , and (d) 1.5  $\mu\text{m}$ .

In order to quantitatively analyze the periodicity of the machined nanostructures, 1D FFT was also selected to conduct the calculation process. The cross-section of the machined structure was utilized to carry out the 1D FFT process. In the measurement process of the machined structure, there are 256 sampling points for one cross-section. The  $x$  coordinate values for these sampling points were mapped to the frequency axis of the amplitude–frequency characteristic diagram obtained by the Fourier transform. The corresponding amplitudes were calculated by Fourier transforming the  $y$  coordinate values for these sampling points. The obtained points in the amplitude–frequency characteristic diagram were connected to form a continuous spectrum, which can be used to quantitatively analyze the periodicity of the machined nanostructures. Due to the variation of the heights of the material pile-ups and the machined depths for the machined structures, the amplitudes shown in the amplitude–frequency characteristic diagrams calculated by the FFT process were different. In order to conduct a quantitative analysis, the obtained amplitudes had to be normalized in the range from 0 to 1.

In this study, we propose an area calculation approach to evaluate the periodicity of the machined nanostructure. The detailed calculation process is as follows: First, the total area between the amplitude–frequency curve obtained by the FFT process and the frequency axis is calculated, and is defined as  $S$ . Next, the peak with the largest amplitude in the amplitude–frequency characteristic diagram is selected; the area between the peak part and the frequency axis is also calculated, and is defined as  $S_1$ . The inflection points close to the frequency axis are chosen as the start and end points for the peak. The ratio,  $\omega$ , of  $S_1$  to  $S$  is employed as a factor to evaluate the periodicity of the machined nanostructure.

To test the proposed method, a sinusoidal curve and a random curve were first selected to implement the periodicity analysis. The sinusoidal curve was obtained by a sinusoidal function of  $y = 2 \sin(2\pi x)$ , as shown in Fig. 7(a); the corresponding normalized amplitude–frequency characteristic diagram is shown in Fig. 7(b). By using the “trapz” function in the Matlab software,  $S$  and  $S_1$  were calculated as 0.251 and 0.251, respectively. Thus,  $\omega$  was equal to 1 in this case. The random curve was obtained by a function of  $y = \text{randperm}(256)$  in the Matlab software, as shown in Fig. 7(c). The normalized amplitude–frequency characteristic diagram for this case is represented in Fig. 7(d), and  $S$  and  $S_1$  were calculated as 3.955 and 0.514, respectively. Thus,  $\omega$  was calculated as 0.039, which is obviously close

to 0. Thus, it can be shown that the larger  $\omega$  is, the better the periodicity of the machined structure is; therefore, the proposed method can be used for the periodicity analysis.

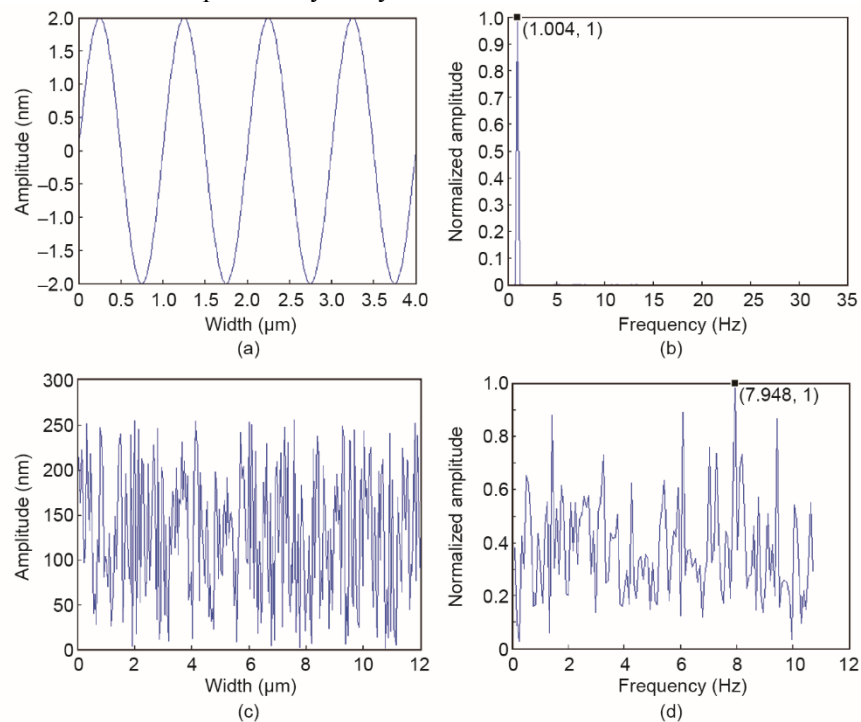


**Fig. 7.** Cross-section and normalized amplitude–frequency characteristic diagram of (a, b) a sinusoidal curve and (c, d) a random curve.

The proposed 1D FFT evaluation method was used to quantitatively analyze the periodicity of the nanostructures shown in Fig. 5. For the cases in which the feed value was less than the total width of the machined groove, the large depth of the groove on the right side of the structure may affect the evaluation process. Thus, in these two cases, the profile of the groove with a relatively large depth was removed from the cross-section of the structure being evaluated by the 1D FFT process, as shown in Fig. 8(a) and (b). The corresponding normalized amplitude–frequency characteristic diagrams are shown in Fig. 8(a) and (b). An obvious peak was found in the normalized amplitude–frequency characteristic diagram, which indicates that the structures machined with the feed values of 0.5  $\mu\text{m}$  and 0.75  $\mu\text{m}$  have a mean frequency spectrum. For the feed value of 0.5  $\mu\text{m}$ ,  $S$  and  $S_1$  were calculated as 0.534 and 0.198, respectively, and  $\omega$  was calculated as 0.371. For the feed value that was enlarged to 0.75  $\mu\text{m}$ ,  $S$  and  $S_1$  were found to be 0.443 and 0.219, and  $\omega$  was calculated as 0.494. This indicates that the nanostructure machined with the feed value of 0.75  $\mu\text{m}$  shows better periodicity than the one machined with the feed value of 0.5  $\mu\text{m}$ . Fig. 8(c) shows the cross-section of the structure scratched with the feed value of 1.27  $\mu\text{m}$ —that is, the total width of the groove and the corresponding normalized amplitude–frequency characteristic diagram. In this case, only one obvious peak was found in the normalized amplitude–frequency characteristic diagram, and the horizontal ordinate of the peak point is 0.837. This reveals that the structure mainly contains one characteristic sinusoidal waveform with a wavelength of 1.2  $\mu\text{m}$ , which is close to the feed value selected in this case.  $S$  and  $S_1$  were calculated as 0.226 and 0.348, respectively, and  $\omega$  was determined to be 0.7366. In this case, the value of  $\omega$  is much closer to 1 than for the structures obtained with feed values less than the total width of the groove. This indicates that the periodicity in this case is better than the periodicity in the cases machined with the feed values of 0.5  $\mu\text{m}$  and 0.75  $\mu\text{m}$ . Fig. 8(d) shows the cross-section of the machined structure and the corresponding normalized amplitude–frequency characteristic diagram for a feed of 1.5  $\mu\text{m}$ . Here, there are three main frequency spectra in the amplitude–frequency characteristic diagram. This reveals that the structure includes three characteristic sinusoidal waveforms. If the peak with the largest value is selected to conduct the evaluation process,  $S$  and  $S_1$  can be calculated as 0.129 and 0.402, respectively, and  $\omega$  is 0.321. However, the structure is not a centrosymmetric sinusoidal waveform, and is therefore different from the cases mentioned above. If the second largest peak is also taken into account,  $S_1$  and  $S_1$  become 0.222 and 0.553, respectively. This indicates that the structure in this case shows good periodicity. Therefore, the methodology proposed in this study can be used effectively to assess the periodicity of the structures.

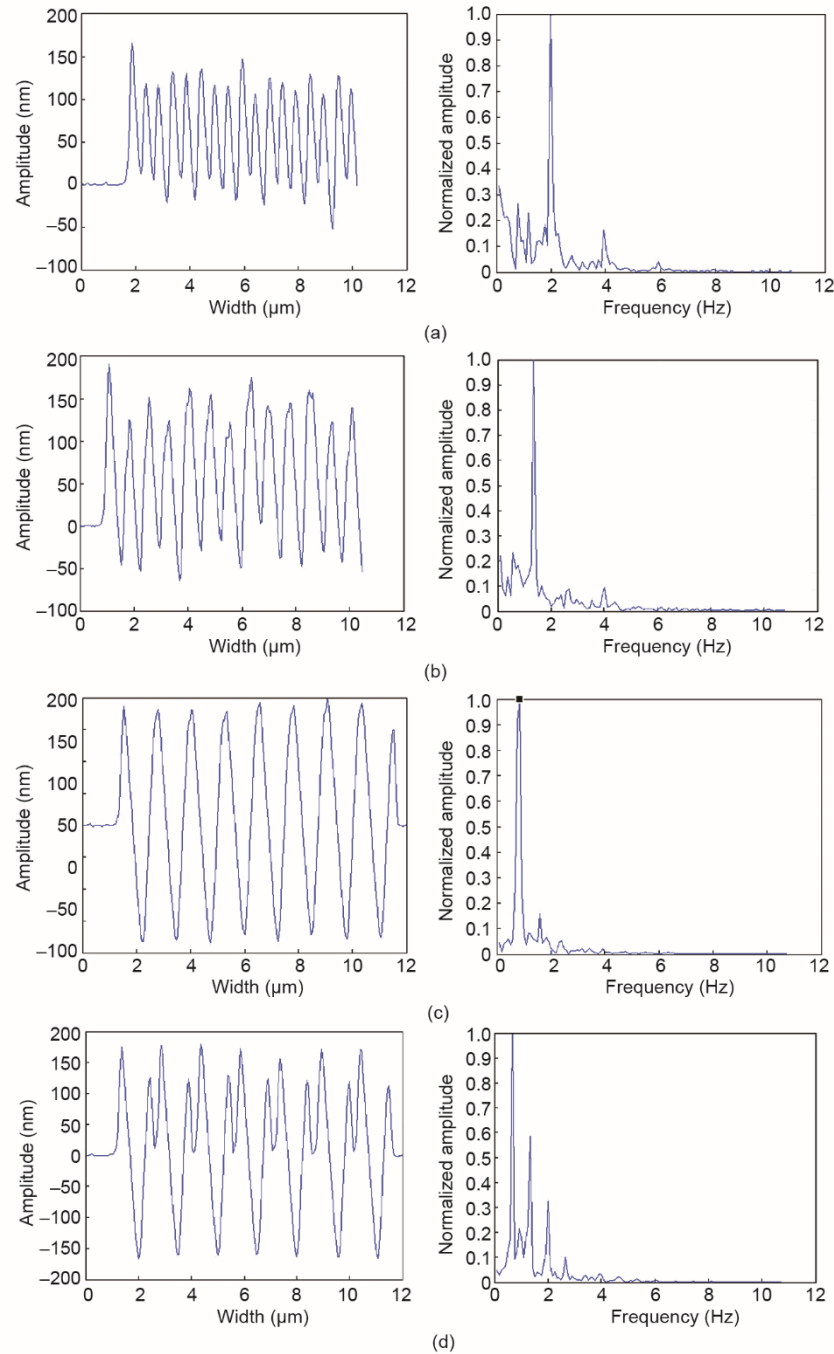


**Fig. 8.** Cross-sections and normalized amplitude–frequency characteristic diagrams for the periodic nanostructures machined with feed values of (a) 0.5  $\mu\text{m}$ , (b) 0.75  $\mu\text{m}$ , (c) 1.27  $\mu\text{m}$ , and (d) 1.5  $\mu\text{m}$ .

### 3.3. Study of the colorization of the machined periodic nanostructure

Periodic near-subwavelength nanostructures on a metallic surface can be employed in various applications, such as color-marking display devices and invisibility cloaks [29–31]. The AFM tip-based approach proposed in this study to create periodic nanostructures has the advantages of low cost, high accuracy, and ease of use, and can be employed to colorize metallic surfaces. When nanoscale patterns are machined to form near-subwavelength structures, the coloration principle is mainly grating diffraction. The relationship between the grating spacing—that is, the period of the structure—and the angle of the diffracted light can be expressed as follows [6]:

$$d(\sin \theta_i + \sin \theta_m) = m\lambda \quad (4)$$

where  $d$  is the grating spacing;  $m$  is the diffraction order, which is an integer and is usually selected as 1;  $\theta_i$  and  $\theta_m$  represent the light incident angle and the diffraction angle of order  $m$ , respectively; and  $\lambda$  is the wavelength of the diffracted light.

When the detection microscope is perpendicular to the surface and the diffraction order is selected as 1, the relationship between the light incident angle  $\theta_i$  and the wavelength of the diffracted light  $\lambda$  can be changed into the following [6]:

$$\theta_i = \arcsin(\lambda/d) \quad (5)$$

Then, based on the period of the structure and the wavelength of the desired light, the light incident angle can be obtained using Eq. (5). In this case, a normal load of 80  $\mu\text{N}$  was selected to fabricate the periodic nanostructure. Based on Eq. (3), a feed value of 1.09  $\mu\text{m}$  was determined to be the value that would yield the structure with the best periodicity. The AFM image of the machined result is shown in Fig. 9, and the corresponding normalized amplitude–frequency characteristic diagram is shown in Fig. 10. In this case,  $S$  and  $S_1$  were calculated as 0.170 and 0.230, respectively, and  $\omega$  was determined to be 0.740, which is similar to the value of  $\omega$  obtained for a feed value of 1.27  $\mu\text{m}$ .

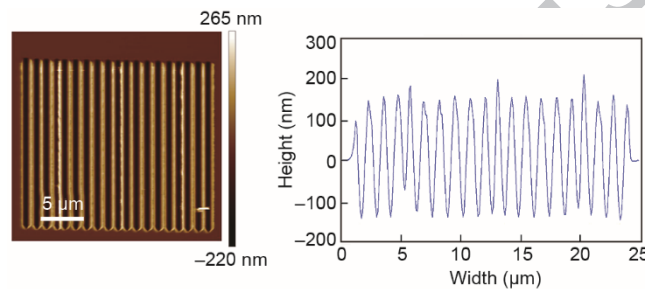


Fig. 9. AFM image and cross-section of the periodic nanostructure machined with a normal load of 80  $\mu\text{N}$  and a feed value of 1.09  $\mu\text{m}$ .

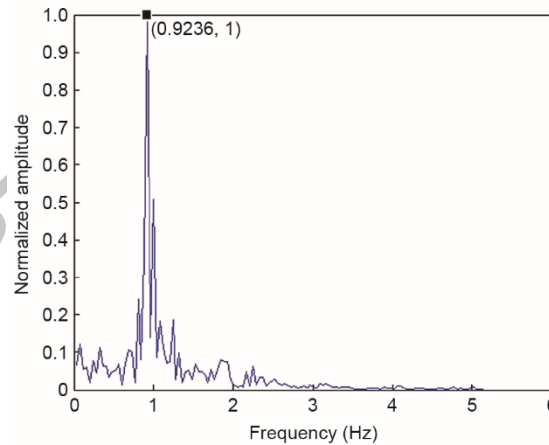
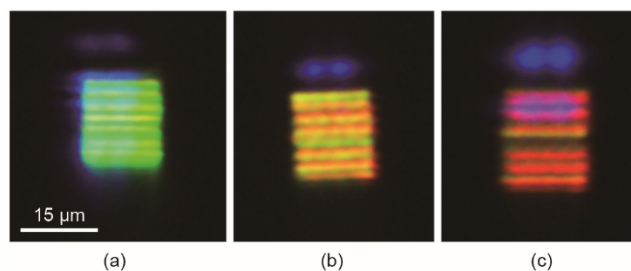


Fig. 10. Normalized amplitude–frequency characteristic diagram of the cross-section shown in Fig. 9.

In this case, the green, yellow, and red color spectra were selected to study the colorization of the machined periodic nanostructures. The wavelength of the green color spectrum ranges from 492 to 577 nm, that of the yellow color spectrum ranges from 577 to 597 nm, and that of the red color spectrum ranges from 622 to 780 nm. Based on Eq. (5), if the wavelength of the received light is 500 nm, 590 nm, and 700 nm, then the corresponding light incident angles can be calculated as 30°, 33°, and 40°, respectively. The resulting color spectra are shown in Fig. 11. Different color spectra can be observed clearly, which agrees well with the calculation results obtained by Eq. (5).



**Fig. 11.** Color spectra obtained by different light incident angles for the structure shown in Fig. 9. (a) 30°; (b) 33°; and (c) 40°.

Two feed values were also selected to fabricate a single structure integrating two different periods. The normal load was again set as 80  $\mu\text{N}$ , and the feed values were chosen as 0.93  $\mu\text{m}$  and 1.09  $\mu\text{m}$ . Fig. 12(a) and (b) shows the AFM image and the corresponding cross-section of the machined structure, respectively. The period of part A in Fig. 12(b) is about 0.9  $\mu\text{m}$ , and the period of part B is about 1.1  $\mu\text{m}$ . When a light incident angle of 33° is selected, the wavelengths of the diffracted light are calculated using Eq. (5) to be about 507 nm for part A and 593 nm for part B; these wavelengths correspond to the green and yellow color spectra, respectively. When the light incident angle is changed to 40°, the wavelengths of the diffracted lights are calculated to be about 597 nm for part A and 700 nm for part B; these wavelengths correspond to the yellow and red color spectra, respectively. The color spectra detected for the light incident angles of 33° and 40° are shown in Fig. 12(c) and (d), respectively. The color spectrum for the structure in the range of part A is shown at the bottom of each image, and that for the structure in the range of part B is shown at the top. The color spectra displayed in Fig. 12(c) and (d) are clearly contrasted, which agrees well with the discussion above.

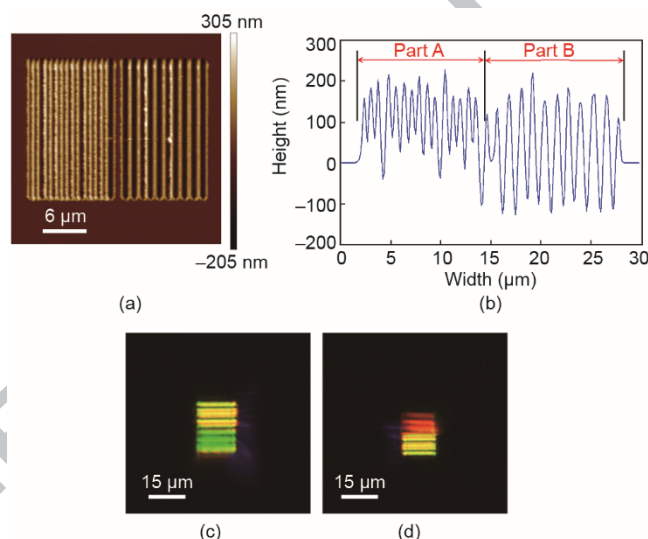


**Fig. 12.** (a) AFM image and cross-section of the structure with two periods; color spectra obtained by light incident angles of (b) 33° and (c) 40°.

Furthermore, the NanoMan module of the AFM instrument was used to fabricate 2D patterns of the abbreviation of Harbin Institute of Technology—that is, “HIT”—with a normal load of 80  $\mu\text{N}$ . A feed value of 1.09  $\mu\text{m}$  was chosen, and the scratching speed was set as 3  $\mu\text{m}\cdot\text{s}^{-1}$ . The dimensions of the pattern are given in Fig. 13(a) and the AFM image of the machined structure is shown in Fig. 13(b). The total scratching length for this 2D pattern can be calculated as 1480  $\mu\text{m}$ , and the total time required for its fabrication was 740 s. This experiment indicates that the method proposed in this study can be used efficiently to fabricate a 2D pattern with a periodic nanostructure. The machined period is around 1.09  $\mu\text{m}$ . Light incident angles of 30°, 33°, and 40° were thus selected in order to obtain the green, yellow, and red color spectra, as shown in Fig. 13(c–e).

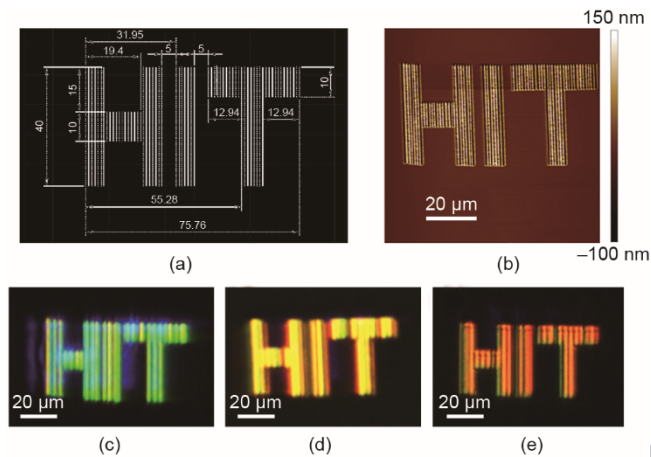


**Fig. 13.** (a) The dimensions and (b) the AFM image of the “HIT” pattern; the color spectra obtained by light incident angles of (c) 30°, (d) 33°, and (e) 40°.

## 6. Conclusions

In summary, nanomachining conducted using an AFM-based nanoscratching system was used to fabricate periodic nanostructures on a single-crystal copper surface by combining the topography from material pile-ups with the topography from machined grooves. The following conclusions were made:

(1) The relationship between the period of the machined structure and the original total width of the groove was examined. When the feed is smaller than the total width of a single groove but much larger than the radius of the tip, the material removed during a subsequent scratch path can partially fill the groove formed by the previous path. In addition, the achieved period for the structure is smaller than the total width of the original groove. When the feed value is larger than the total width of the groove, the adjacent scratch paths cannot be overlapped. When the feed value is equal to the total width of the groove, the adjacent material pile-ups can connect exactly with each other and the machined structure shows acceptable periodicity.

(2) The periodicity of the machined structure was evaluated using 1D and 2D FFT algorithms. From the 2D FFT results, it was concluded that structures machined with a feed value equal to the total width of a single groove show better periodicity. Next, based on the 1D FFT result, the ratio of the area of the peak part to the total area in the normalized spectral graph of the cross-section of the structure was used to quantitatively analyze the periodic nanostructures. The obtained results agreed well with the 2D FFT analysis.

(3) The colorization of the machined periodic nanostructure was studied in order to demonstrate the potential of this method for anti-counterfeiting and metal sensor applications. Based on the period of a machined structure and the wavelength of the desired color spectrum, the light incident angle can be set. Different color spectra can then be obtained successfully by changing the light incident angle.

The AFM tip-based approach proposed in this study has the advantages of low cost, high accuracy, and ease of use when compared with other nanomanufacturing methods for fabricating periodic nanostructures; however, this approach is still in its infancy with respect to potential industrial applications. The most critical issue that needs to be solved is the significant tip wear that occurs after long-distance scratching, which will greatly reduce the machining accuracy. Further studies should be carried out to consider combining a high-frequency vibration machining technique or a lubricant with the proposed method in order to reduce the tip wear when conducting long-distance scratching.

## Acknowledgements

The authors gratefully acknowledge financial support from the National Natural Science Foundation of China (51705104, 51475108, and 51675134), the Foundation for Innovative Research Groups of the National Natural Science Foundation of China (51521003), the Key Laboratory of Micro-systems and Micro-structures Manufacturing of the Ministry of Education, Harbin Institute of Technology (2017KM005), and the National Program for Support of Top-Notch Young Professors

## Compliance with ethics guidelines

Yanquan Geng, Yongda Yan, Jiqiang Wang, Emmanuel Brousseau, Yanwen Sun, and Yazhou Sun declare that they have no conflict of interest or financial conflicts to disclose.

## References

- [1] Ali M, Zhou F, Chen K, Kotzur C, Xiao C, Bourgeois L, et al. Nanostructured photoelectrochemical solar cell for nitrogen reduction using plasmon-enhanced black silicon. *Nat Commun* 2016;7:11335.
- [2] Wei WR, Tsai ML, Ho ST, Tai SH, Ho CR, Tsai SH, et al. Above-11%-efficiency organic-inorganic hybrid solar cells with omnidirectional harvesting characteristics by employing hierarchical photon-trapping structures. *Nano Lett* 2013;13(8):3658–63.
- [3] Zhao Z, Shin SH, Choi DG, Park SH, Jeong JH. Shape-controlled 3D periodic metal nanostructures fabricated via nanowelding. *Small* 2017;14(6):1703102.
- [4] Hu M, Chen J, Li Z, Au L, Hartland GV, Li X, et al. Gold nanostructures: engineering their plasmonic properties for biomedical applications. *Chem Soc Rev* 2006;35(11):1084–94.
- [5] Mulvihill MJ, Ling X, Henzie J, Yang P. Anisotropic etching of silver nanoparticles for plasmonic structures capable of single-particle SERS. *J Am Chem Soc* 2010;132(1):268–74.
- [6] Yang Y, Pan Y, Guo P. Structural coloration of metallic surfaces with micro/nano-structures induced by elliptical vibration texturing. *Appl Surf Sci* 2017;402:400–9.
- [7] Vorobyev AY, Guo C. Colorizing metals with femtosecond laser pulses. *Appl Phys Lett* 2008;92(4):041914.
- [8] Yao J, Le AP, Schulmerich MV, Maria J, Lee TW, Gray SK, et al. Soft embossing of nanoscale optical and plasmonic structures in glass. *ACS Nano* 2011;5(7):5763–74.
- [9] Xu ZW, Fang FZ, Fu YQ, Zhang SJ, Han T, Li JM. Fabrication of micro-/nano-structures using focused ion beam implantation and XeF<sub>2</sub> gas-assisted etching. *J Micromech Microeng* 2009;19(5):054003.
- [10] Yan Y, Geng Y, Hu Z. Recent advances in AFM tip-based nanomechanical machining. *Int J Mach Tools Manuf* 2015;99:1–18.
- [11] Zhan D, Han L, Zhang J, Shi K, Zhou J, Tian Z, et al. Confined chemical etching for electrochemical machining with nanoscale accuracy. *Acc Chem Res* 2016;49(11):2596–604.
- [12] Tseng AA. Advancements and challenges in development of atomic force microscopy for nanofabrication. *Nano Today* 2011;6(5):493–509.
- [13] Deng J, Zhang L, Dong J, Cohen PH. AFM-based 3D nanofabrication using ultrasonic vibration assisted nanomachining. *J Manuf Process* 2016;24:195–202.
- [14] Garcia R, Knoll AW, Riedo E. Advanced scanning probe lithography. *Nat Nanotechnol* 2014;9(8):577–87.
- [15] Yan Y, Geng Y, Hu Z, Zhao X, Yu B, Zhang Q. Fabrication of nanochannels with ladder nanostructure at the bottom using AFM nanoscratching method. *Nanoscale Res Lett* 2014;9(1):212.
- [16] Pires D, Hedrick JL, De Silva A, Frommer J, Gotsmann B, Wolf H, et al. Nanoscale three-dimensional patterning of molecular resists by scanning probes. *Science* 2010;328(5979):732–5.
- [17] Chen CF, Tzeng SD, Chen HY, Gwo S. Silicon microlens structures fabricated by scanning-probe gray-scale oxidation. *Opt Lett* 2005;30(6):652–4.
- [18] Guo J, Yu B, Chen L, Qian L. Nanodestructive nanofabrication on Si (100) surface by tribochemistry induced selective etching. *Sci Rep* 2015;5(1):16472.
- [19] Yan Y, Hu Z, Zhao X, Sun T, Dong S, Li X. Top-down nanomechanical machining of three-dimensional nanostructures by atomic force microscopy. *Small* 2010;6(6):724–8.
- [20] Geng Y, Yan Y, Xing Y, Zhao X, Hu Z. Modelling and experimental study of machined depth in AFM-based milling of nanochannels. *Int J Mach Tools Manuf* 2013;73:87–96.
- [21] Geng Y, Yan Y, Brousseau E, Sun Y. AFM tip-based mechanical nanomachining of 3D micro and nano-structures via the control of the scratching trajectory. *J Mater Process Technol* 2017;248:236–48.
- [22] Geng Y, Yan Y, Brousseau E, Cui X, Yu B, Zhao X, et al. Machining complex three-dimensional nanostructures with an atomic force microscope through the frequency control of the tip reciprocating motion. *J Manuf Sci Eng* 2016;138(12):124501.
- [23] Geng YQ, Yan YD, Zhao XS, Hu ZJ, Liang YC, Sun T, et al. Fabrication of millimeter scale nanochannels using the AFM tip-based nanomachining method. *Appl Surf Sci* 2013;266:386–94.
- [24] Kawasegi N, Takano N, Oka D, Morita N, Yamada S, Kanda K, et al. Nanomachining of silicon surface using atomic force microscope with diamond tip. *J Manuf Sci Eng* 2006;128(3):723–9.
- [25] He Y, Yan Y, Geng Y, Brousseau E. Fabrication of periodic nanostructures using dynamic plowing lithography with the tip of an atomic force microscope. *Appl Surf Sci* 2018;427:1076–83.
- [26] Geng Y, Zhang J, Yan Y, Yu B, Geng L, Sun T. Experimental and theoretical investigation of crystallographic orientation dependence of nanoscratching of single crystalline. *Plos One* 2015;10(7):e0131886.
- [27] Dongmo LS, Villarrubia JS, Jones SN, Renegar TB, Postek MT, Song JF. Experimental test of blind tip reconstruction for scanning probe microscopy. *Ultramicroscopy* 2000;85(3):141–53.
- [28] Tseng AA, Kuo CFJ, Jou S, Nishimura S, Shirakashi J. Scratch direction and threshold force in nanoscale scratching using atomic force microscopes. *Appl Surf Sci* 2011;257(22):9243–50.
- [29] Dusser B, Sagan Z, Soder H, Faure N, Colombier JP, Jourlin M, et al. Controlled nanostructures formation by ultra fast laser pulses for color marking. *Opt Express* 2010;18(3):2913–24.
- [30] Liu J, Coleman JP. Nanostructured metal oxides for printed electrochromic displays. *Mater Sci Eng A* 2000;286(1):144–8.
- [31] Ergin T, Stenger N, Brenner P, Pendry JB, Wegener M. Three-dimensional invisibility cloak at optical wavelengths. *Science* 2010;328(5976):337–9.